

14. Electron scattering from unstable nuclei with the SCRIT

(abstract)

Research goal of this proposal is to determine nuclear charge distribution of short-lived isotopes by elastic electron scattering experiment. We propose a new method of electron scattering experiment for unstable nuclei using the SCRIT. The SCRIT (Self-Confining Radioactive Ion Target) is the trapped-ion cloud formed at a local position in an electron storage ring, and is used as a target of the electron scattering experiments. Ions are three-dimensionally confined in the transverse focusing kick given by the projectile electron beam itself and additionally applied longitudinal mirror potential. RI ions are injected into the SCRIT from outside, so we need slow RI ion source like an ISOL. In our numerical calculation, the luminosity of e-RI collision is achievable to be more than $10^{28} \text{ s}^{-1} \text{ cm}^{-2}$. The experimental system consists of an electron linac, an electron storage ring with the SCRIT device, a slow RI beam generator (ISOL), and a detector system. The R&D study of the SCRIT technology is now underway at the KSR (Kyoto SOR Ring), and the feasibility has been confirmed.

CONTENTS

- I. List of collaborations
- II. Physics subject to be investigated and observables to be measured
- III. Experimental devices
 - III-1. SCRIT
 - III-2. Electron beam accelerators
 - III-3. Electron storage ring
 - III-4. RI generator, ISOL, and ion injection system
 - III-5. Detector system
 - III-5-1. Requirements
 - III-5-2. Detector design concept
 - III-5-3. Electron Detection Arm
 - III-5-4. Recoiled particle detector
 - III-5-5. Luminosity Monitor
 - III-6. Further recycling plan
- IV. R&D study of the SCRIT
- V. Costs
 - V-1. Cost of the minimum plan
 - V-2. Cost of additional high-power electron linac for RI production
 - V-3. Cost of full specification with recycling of the KSR and its injector linac
- VI. Time table of construction, budgets, and staffs
- References

I. LIST OF COLLABORATORS

Spokesperson:

M. Wakasugi* (*Cyclotron Center, RIKEN*)

Collaborators:

T. Emoto (*Cyclotron Center, RIKEN*)

S. Ito (*Cyclotron Center, RIKEN*)

T. Koseki (*Cyclotron Center, RIKEN*)

K. Kurita (*Department of Physics, Rikkyo University*)

M. Nakamura (*Cyclotron Center, RIKEN*)

T. Suda (*Heavy Ion Nuclear Physics Lab., RIKEN*)

T. Tamae (*Laboratory of nuclear Science, Tohoku University*)

H. Takeda (*RI Physics Lab., RIKEN*)

Y. Yano (*Cyclotron Center, RIKEN*)

II. PHYSICS SUBJECTS TO BE INVESTIGATED AND OBSERVABLES TO BE MEASURED

Among various probes to investigate the internal nuclear structure, electron scattering is one of the best probe. Thanks to electromagnetic coupling between electron and a target nucleus, one can extract the internal structure information unambiguously from experimental data. Due to obvious lack of a solid target for short-lived unstable nucleus, however, no electron scattering has ever been performed for those nuclei.

We propose to construct electron scattering facility at the RI Beam Factory [YA04] to study the internal structure, mainly charge distribution, of many short-lived radioactive isotopes (RI). Research goal of this proposal is to determine the charge distribution of short-lived nuclei precisely by electron scattering [TA95]. The precise determination of such density distribution of unstable nuclei provides a critical test of our understanding of their internal structure. As is well known, the charge distribution is determined from the differential cross section for elastic electron scattering. The observables we will measure are the differential cross section as a function of the electron scattering angle, i.e. momentum transfer. The numerical simulations have demonstrated that one may determine the diffraction radius and surface diffuseness of a target nuclei with the luminosity of $10^{28}/\text{cm}^2/\text{s}$ and one-week measurement [SU05].

The matter distribution will be also determined by proton elastic scattering experiments at RIBF [TA03]. Combining the matter distribution determined by the proton elastic scattering, one may be able to separately determine the proton- and neutron-distribution. Such information will be the basic input for formulating a universal picture of the nuclear structure applicable not only for stable nuclei but also nuclei far from stability.

III. EXPERIMENTAL DEVICES

The conventional way of the electron scattering experiment for unstable nuclei is a collider scheme, which consists of an electron storage ring including an electron accelerator and a large ion storage ring with large acceptance and cooling devices to achieve necessary luminosity. The SCRIT system does not need the ion storage ring. Schematic drawing of the experimental system with the SCRIT is shown in Fig. III-1. This system consists of an electron beam accelerator, a small electron storage ring with the SCRIT device, a slow RI beam generator, and detector system for scattered electron and recoiled ions. By using the SCRIT, the physical space and cost required for the whole system is estimated to be about 10% compared with the collider scheme.

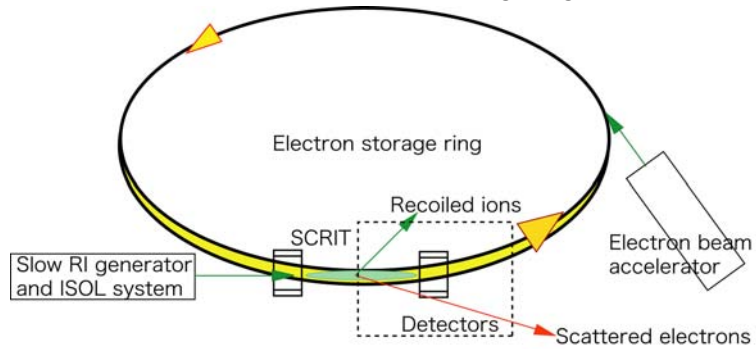


Fig. III-1. Schematic view of the electron scattering system with the SCRIT.

A plan of the experimental system is shown in Fig. III-2.

Considering cost performance, a 150-MeV microtron is adopted as an electron beam injector to the storage ring. The small electron beam storage ring will be recycled of the NIJI-II, which is an existing machine at National Institute of Advanced Industrial Science and Technology (AIST). An ISOL system with an ion source and the ion injection line will be newly constructed. The detector system consists of the scattered electron detector, recoiled ion detector, and luminosity monitors.

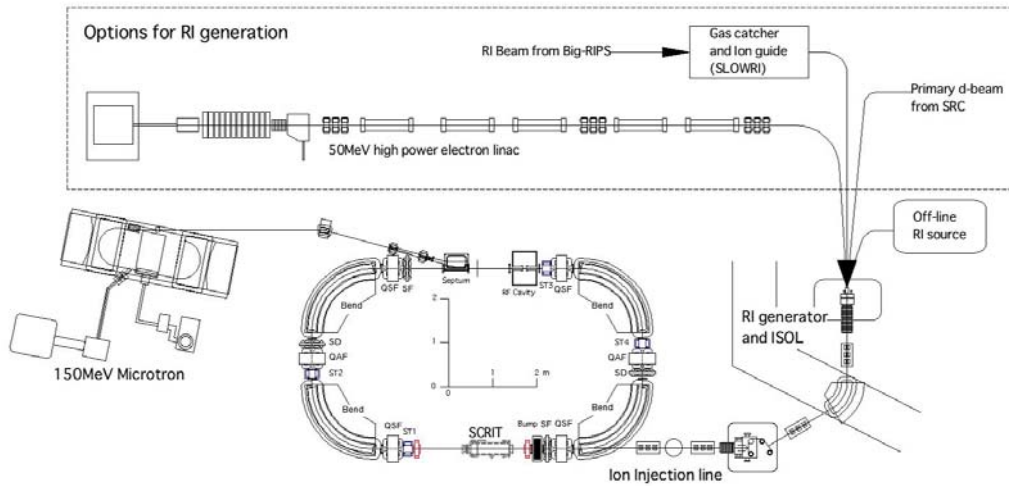


Fig. III-2. Experimental system planned for the electron scattering with the SCRIT. In the first phase the RI generator will be used off-line. There are some options shown in the square for on-line RI production in next phase.

There are several methods to supply RI's to the ion source. When we use uranium-fission to produce RI's at the ion source, a high-power electron linac and/or primary d beam from the SRC are possible choices as a driver. A slow RI beam extracted from a gas catcher and ion guide system (SLOWRI) can also be used as an RI source. They are options in advanced course. In the first phase, we will construct the minimum plan, in which the RI generator will be used off-line, shown in the figure. Details for each device are described follows.

III-1. SCRIT

The SCRIT (Self-Confining Radioactive Ion Target) technology provides a fixed RI ion target for electron scattering experiment. The RI ions are three-dimensionally confined along the electron beam axis in the storage ring. This confinement is realized by periodic transverse focusing kick by the electron bunches and additionally applied longitudinal mirror potential at a local position of the electron storage ring (see Fig. III-1-1). This is the combination of the EBIT(EBIS) technology [DO76,AR76,PE91] and "ion trapping" phenomenon [LA74,BA86,BO89] in the electron storage ring.

Since the SCRIT is a completely new device, we should study its performance. First we made computer simulation on the ion motion in the SCRIT [WA04]. Purpose of the numerical simulation is to expect how long ions lives in the SCRIT, how many ions can be trapped, and how much luminosity can be obtained. We calculate particle motion and their time evolution in superposition of three kinds of electro-magnetic fields, which are the time-dependent negative potential coming periodically created by electron bunch, longitudinal mirror potential given by the SCRIT electrodes, and positive potential depending on the spatial distribution of trapped ion cloud.

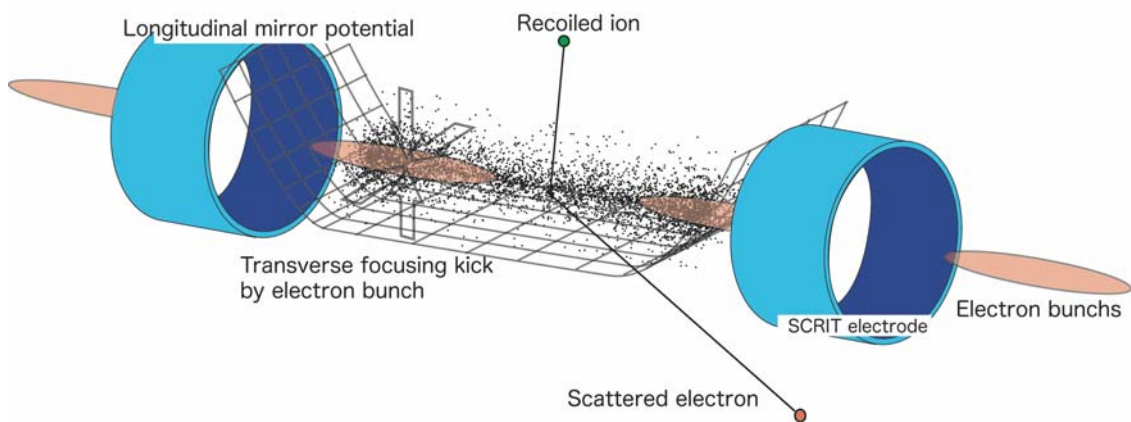


Fig. III-1-1. Principal of the SCRIT

Many kinds of physical processes are taken into accounts in this calculation, for example, electron impact ionization, ion heating by Coulomb collision, nuclear decay, etc. Figure III-1-2 shows time evolution of number of ^{132}Sn ions, which are injected into the SCRIT from outside, in the SCRIT. The time evolutions obtained here are confirmed with the Penetrante's method [PE91], which is well-established calculation in the EBIS (EBIT) field. This calculation tells us that 10^7 - 10^8 ions is acceptable at the SCRIT, of which the length is 130 mm, the lifetime of the SCRIT is order of second when the electron beam current is several hundreds mA.

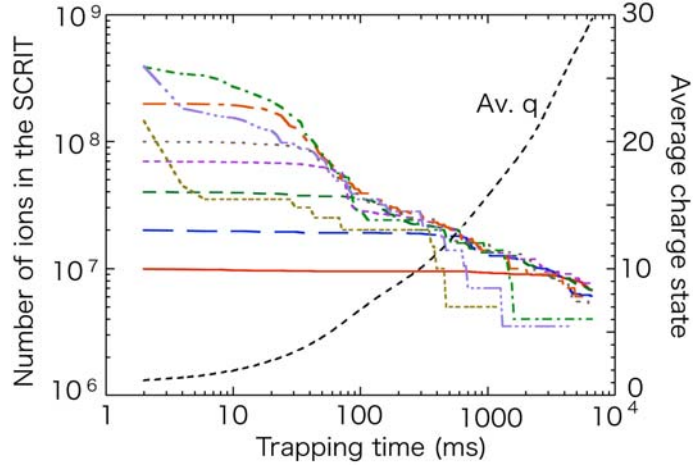


Fig. III-1-2. Calculated time evolution of number of trapped ions in the SCRIT. Decay curves are plotted for several cases of the number of initially injected ions (N_{inj}), and the averaged charge state (Av.q) at vacuum pressure of 10^{-7} Pa is also plotted.

Since the time evolution is a function of number of initially injected ion (N_{inj}), the ion injection should be repeated with an appropriate period (τ_{cycle}) to maintain the required luminosity during measurement. So the luminosity L is a function of the N_{inj} and the τ_{cycle} . In case of short-lived isotope intrinsic lifetime (τ_{life}) has to be considered. Then the time-averaged luminosity L is defined as

$$L_{\tau_{life}}(N_{inj}, \tau_{cycle}) = \frac{1}{\tau_{cycle}} \int_0^{\tau_{cycle}} L_{\infty}(N_{inj}, \tau_{cycle}) \exp\left(-\frac{t}{\tau_{life}}\right) dt \quad ,$$

where $L_{\infty}(N_{inj}, \tau_{cycle})$ is calculated with the simulation described above. The N_{inj} is a function of the RI production rate (R_{prod}) and the injection efficiency (ε_{inj}). Figure III-1-3 shows achievable luminosity with $\varepsilon_{inj} = 0.1\%$ as a function of the R_{prod} . The time-averaged luminosity of more than $10^{27} \text{ cm}^{-2}\text{s}^{-1}$ is achievable, when we repeat the injection and the release of ions in the SCRIT with a period of 1-2 sec.

Comparing with the collider scheme, advantages of the SCRIT scheme are

- (1) Small space and low cost.
- (2) Synchronization between the electron beam and ion beam is not needed because the electron beam itself holds the target ions.
- (3) All trapped ions always participate to the collision, which may result higher luminosity.
- (4) Cooling devices are unnecessary.
- (5) Recoiled ions are detectable because target ions are floated in the free space with nearly zero energy compared with the electron beam.
- (6) Since detection of the recoiled ions is helpful in the determination of the scattering kinematics, telescopic detection of the scattered electron is possible and a 4π -detector can be easily designed.

(7) Since the recoiled ions can be identified by means of TOF (velocity of recoiled ion) measurement and detection of γ ray due to nuclear decay, background caused by residual gas ion and daughters are completely suppressed.

The R&D study to confirm the SCRIT principal is now under way at the KSR in Kyoto University. Details are described in chapter IV.

III-2. Electron Beam Accelerator

In our minimum plan, the electron beam accelerator for injection into the storage ring will be a 150-MeV microtron. Optionally a 50-MeV high-power electron linac will be used as a driver for RI generation (see section III-4). The injector 150-MeV microtron is commercially available in Sumitomo Heavy Industry. This is a racetrack type of microtron and developed as an injector for a small storage ring. The system includes the 120-keV injector. This is a compact machine as shown in Fig. III-2 and the emittance and the momentum spread of output beam are ten times smaller than those of the linac. This has higher cost performance than the linac, which has the same acceleration energy. Specifications of the microtron are listed in Table III-2-1. Peak current is less than the linac, but it is enough as an injector.

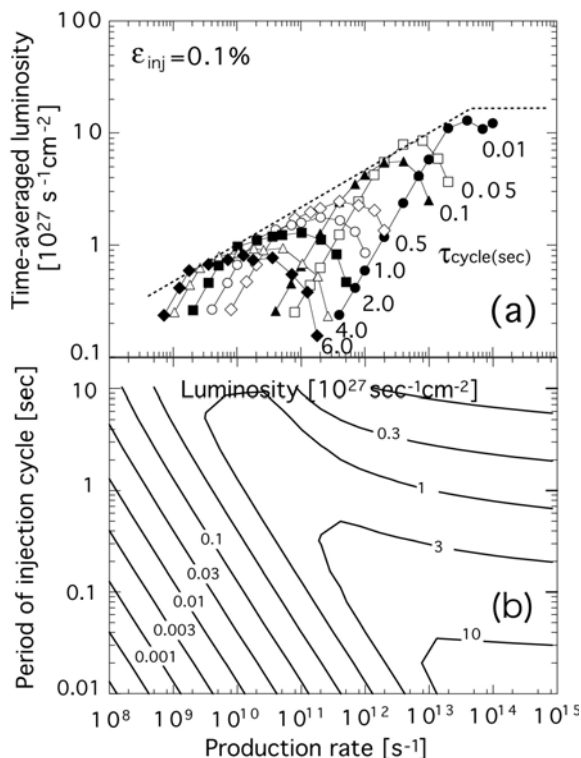


Fig. III-1-3. Estimated achievable luminosity.

Table III-2-1. Specifications of the 150-MeV microtron

Max. magnetic field	1.23	T
Injection energy	120	keV
Final energy	150	MeV
Energy gain	6.0	MeV/turn
Number of orbit	25	turns
Beam current	15	mA
Repetition rate	1-180	Hz
Emittance (ϵ_x/ϵ_y)	0.6 / 0.4	π mm mrad
Energy spread	0.1	%
RF frequency	2856	MHz
Pulse width	6	μs

Field gradient	15	MeV/m
Klystron power	5.5	MW

If we choose the electron beam as a driver for RI production on the UC₂ target at the ion source, machine choice is a 50-MeV high-power (50kW average beam power) electron linac based on the industrial radiation processing. This is the S-band (2856 MHz) linac, its acceleration scheme is linear combination of an electron gun, a pre-buncher, a buncher, and five acceleration tubes, which are S-band standing-wave type of accelerating tubes. Specifications of the electron linac are listed in Table III-2-2. This linac is also commercially available and there is no serious technical problem.

Fig. III-2-2. Specifications of the 50-MeV driver linac.

Linac performance	Energy	50MeV
	Accelerating gradient	~10MeV/m
	Beam current	250mA
	Pulse width	16 μ s
	Pulse repetition	250pps
	Average beam power	50kW
Electron gun	Type	Triode
	Energy	25keV
	Beam current	300mA
Acceleration section	Number of sections	5
	Length	1.2m
	Field mode	$\pi/2$
	Wave type	Standing wave
	Frequency	2856 \pm 1MHz
	RF feed power	~4.7MW/section
RF power units	Klystron power (max)	5MW
	Pulse width	~17 μ s
	Number of klystrons	1/section
	Number of units	5

III-3. Electron Storage Ring

The storage ring for SCRIT experiment will be constructed by recycling of the NIJI-II ring, which is a second-generation synchrotron radiation source constructed in 1988 at National Institute of Advanced Industrial Science and Technology (AIST). The original NIJI-II ring is a four-dipole racetrack type of ring with two 2-m straight sections and circumference of 17 m. The injection and maximum beam energies are 150 and 600 MeV, respectively. Although the storage ring for SCRIT is assumed to be the NIJI-II ring,

some modifications are required to be suitable for the electron scattering experiment. The main modifications will be as follows;

- (1) Two straight sections of the ring will be extended from 2 m to ~3.5 m in order to make spaces for the SCRIT system including detectors and the other accelerator components, such as steering magnets and beam monitors.
- (2) Control system will be renewed to unify the injector and ring control.
- (3) Power supplies of magnets will be renewed.
- (4) Power source of rf system will be changed from tetrode tube to solid state power amplifier.

Parameters of the ring, which is redesigned for the SCRIT use, are listed in Table III-3-1. The lattice structure, beta functions and dispersion are shown in Fig. III-3-1(a) and (b). This ring is dispersive over the whole ring, but it is not a problem for the SCRIT so far as serious longitudinal instability dose not appear.

Table III-3-1. Machine parameters of the electron storage ring.

Circumference		20.84656	m
Length of straight section		3.356	m
Bending magnet	Radius	1.4	m
	Edge angle	+16.0	Deg.
Quadrupole magnet	QAF	1.22926	/m ²
	QSF	0.156778	/m ²
Sextupole magnet (for chromaticity correction)	SD	-25.429	/m ³
	SF	23.314	/m ³
Tune	Q _x / Q _y	1.370/0.6028	
Momentum Compaction	α	0.4857	
Transition gamma	γ _t	1.4348	
Maximum beta function	β _x / β _y	4.96 / 6.44	m
Maximum dispersion	D _x / D _y	1.88/0.0	m
Chromaticity	ξ _x / ξ _y	-1.09/-0.34	
Electron beam parameters			
Energy (injection/operation)	E	150/300	MeV
Radiation loss (at 150MeV)	U ₀	31.99	eV/turn
Equilibrium emittance	ε _x /ε _y	38.8 / 56.0	π n m rad
Natural energy spread	ΔE/E	8.9 × 10 ⁻⁵	
Damping time	τ _x / τ _y / τ _e	12.5/0.65/0.22	sec
Beam size	σ _x / σ _y	0.43/0.56	mm
Natural bunch length	σ _s	31.7	mm
Revolution time	T ₀	69.5	nsec

Touschek lifetime (at $E=150\text{MeV}$, $V_{rf}=30\text{kV}$)	τ_{tous}	20	min
RF frequency	f_{RF}	158.19	MHz
Harmonic number	h	11	
Maximum RF voltage	V_0	30	kV

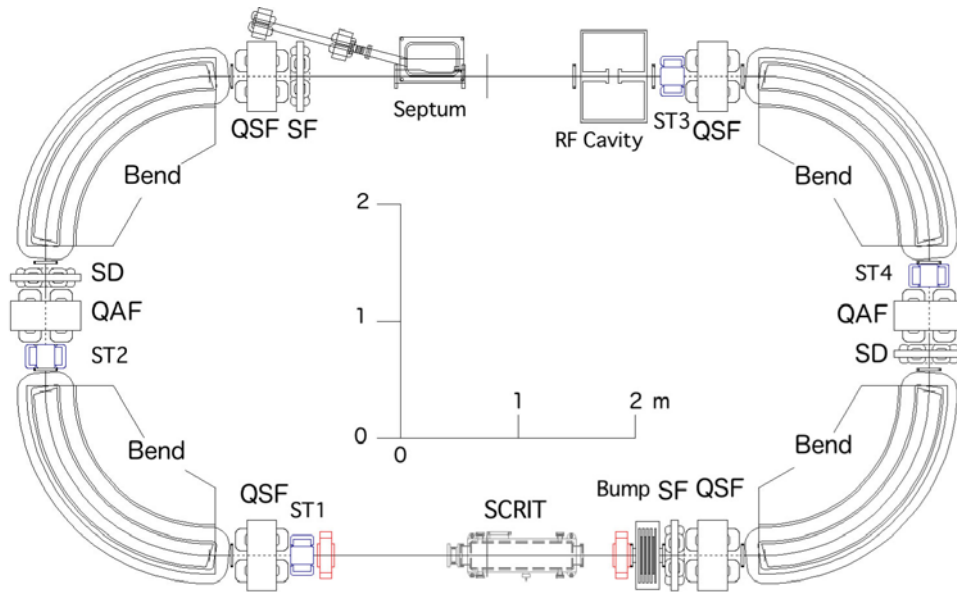


Fig. III-3-1(a). Lattice structure of the electron storage ring for SCRIT.

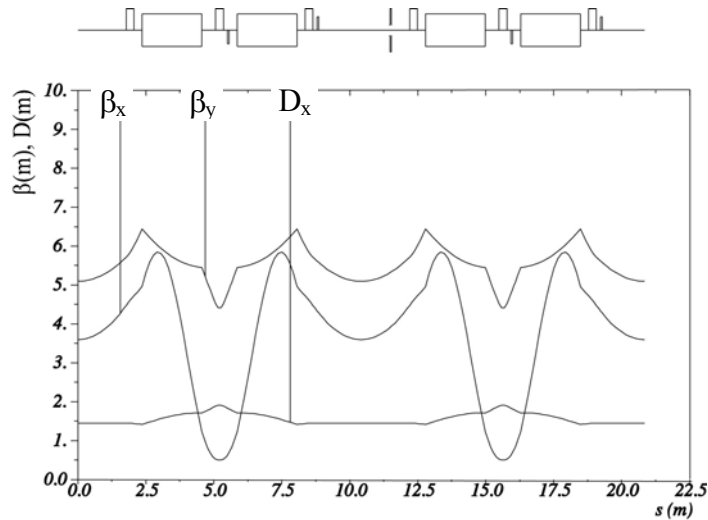


Fig. III-3-1(b). Beta functions and dispersion function of the electron storage ring for SCRIT.

In the original design of the NIJI-II, the stored current was 300 mA at the beam energy of 150 MeV, and the lifetime was several hours. These are nearly desired performances for the SCRIT experiment. Important characteristics, which give high performances, are the large dynamic aperture and long

Touschek lifetime. Large dynamic aperture and long Touschek lifetime are designed in our ring to achieve large accumulation current and long lifetime. From tracking simulations, much larger dynamic aperture than the physical aperture is obtained as shown in Fig. III-3-2. The Touschek lifetime depends on the stored current and is affected by the intra beam scattering. The bunch length, energy spread, and

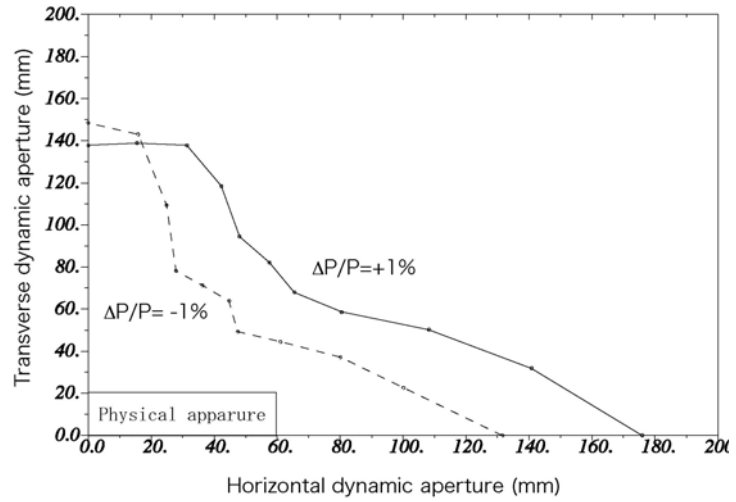


Fig. III-3-2. Calculated dynamic aperture.

emittance grow up with the current. Taking these effects into account the estimated Touschek lifetimes for the beam energy of 150 MeV and 300 MeV are shown in Fig. III-3-3. For instance, the Touschek lifetime at the injection energy can be longer than the time for injection process, and it is several tenth minutes at the top energy. The Touschek lifetime is expected to be longer than this calculation, because intra beam scattering will be reduced by the growth of the bunch length and the momentum spread due to microwave instability caused by the broadband impedance.

Present modification is minimized so as to maintain the characteristics of the lattice such as weak focusing, fully dispersive, etc. Therefore, there is no serious difficulty in the modification. Performances expected from our machine design are not much different from original ones. The rf system, control system, and power supplies of magnets should be renewed, because they are old-fashioned. The other requirements for reconstruction of NIJI-II are renewals of an evacuation system and some vacuum chambers.

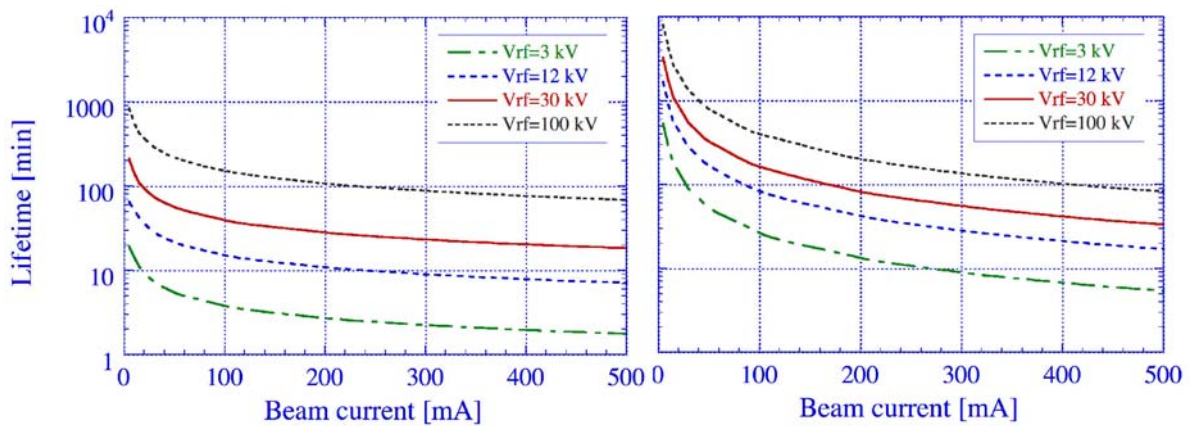


Fig. III-3-3. Touschek lifetime as a function of beam current for several case of the rf voltage.

III-4. RI Generator, ISOL, and ion injection system

Ion beam supply to the SCRIT is separated into two parts; an RI generator connected to an ISOL system and ion injector including a pulse ion source. A slow and good-quality RI beam of interest is supplied from an RI beam generator, which is directly connected to a DC ion source in an ISOL system. Several kinds of ion source can be used such as a surface-ionization, a plasma ion source, and an ECR ion source, as the DC ion source. They will be used according to chemical characteristics of RI's of interest. Ions from the source are accelerated to 50 keV and mass-separated by an analyzing magnet. The mass resolution of $M/\Delta M=300$ is enough and we do not need high resolution such as to an isobar separator, because identification of the recoiled ions is possible in electron scattering measurement that is one of big advantages of the SCRIT. The separated ions of interest are transported to the ion injection system including a pulse ion source and stacked here for an injection period (τ_{cycle}). They are extracted as a pulsed ion beam at a pulse length of less than $100\mu s$, transported to the electron storage ring with about 10-keV energy and injected into the SCRIT. Here the ion beam emittance is limited by the SCRIT acceptance. The potential depth produced by the electron beam determines the SCRIT acceptance. This is typically 30π mm mrad at nS electron beam current of a few hundreds mA. The ion beam size at the merging point with the electron beam is desirable to be the same size with the electron beam. These requirements, which are low emittance and low energy spread, are not technically easy for the pulsed ion source. The beam quality influences the injection efficiency and the achievable luminosity as shown in Fig. III-1-3. The high-quality slow-ion-beam generation is important task, which should be studied.

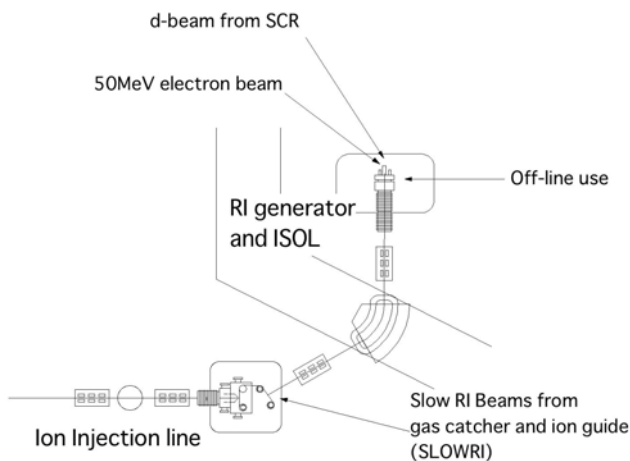


Fig. III-4-1. Principal of the RI generation and ion injection scheme.

In the minimum plan, we will use this system off line, and the target RI will be unstable nuclei with rather long lifetime. In on-line use in future we have several choices to supply RI's to the system as described above. One possibility is a use of a gas catcher system with an rf ion guide (SLOWRI) connected to a projectile fragment separator. In this case the slow RI beams from the SLOWRI are injected directly into the ion injection system. Recently the possibility to obtain high yields of uranium fission fragments such as ^{132}Sn has been reported, where high-intensity neutrons or photons bombard the UC_2 target [AL99,WE01,DI99]. Photons are produced through Bremsstrahlung driven by a high power electron beam described above. The fission rate in the target is estimated to be 5×10^{11} fissions/s and the production rate of ^{132}Sn is about 10^9 /s per 1-kW electron beam power. The ion source at the RI generator

consists of a radiator plate, UC₂ target in a high-temperature oven, and ionizer connected to the oven. The electron beam is converted to the Bremsstrahlung γ -ray at the radiator plate and the γ -ray radiates the UC₂ target. Fissions of the U nucleus inside the target produce the short-lived neutron-rich isotopes in the mass region of 90-140. Since the UC₂ target has porous structure, produced RI's are quickly released with a high release rate. The other possibility to produce RI's is to use a deuteron beam from the SRC as a driver of U fission process at the RI generator.

III-5. Detector system

III-5-1 Requirements

The advantages of electron scattering for the nuclear-structure studies are summarized as follows;

- (1) The electromagnetic coupling constant is weak enough to use the Born approximation, and to allow us to probe the whole volume of a nucleus.
- (2) The electron-nucleus interaction is well described by QED, which enables us to extract structure information unambiguously from the experimental data.
- (3) The three-momentum transfer, q , can be varied independently of the energy transfer, ω , which maps out the Fourier component of a particular transition matrix element.

Since the charge distribution of unstable nuclei is the main subject, we focus only on *elastic* electron scattering. First of all, the elastic-scattering cross section has the Z^2 -dependence. It is the largest among those for the other scattering processes, up to moderate momentum transfer, because of a coherent contribution of all protons in a nucleus to elastic scattering.

The differential cross section for elastic scattering from a spin-less nucleus under a Plane-Wave Impulse-Approximation (PWIA) is given as [DE66],

$$\left. \frac{d\sigma}{d\Omega} \right]_{elastic} = \sigma_{Mc} |F_c(q)|^2,$$

where σ_{Mc} is the Mott cross section, and $F_c(q)$ is the charge form factor. The Mott cross section is the elastic-scattering cross section from a point particle of charge Z .

$$\sigma_M = \frac{(Z\alpha)^2 \cos^2\left(\frac{\theta}{2}\right)}{4E_e^2 \sin^4\left(\frac{\theta}{2}\right)},$$

where E_e is electron energy, θ the scattering angle and α the fine-structure constant.

The form factor is a Fourier component of the charge distribution, $\rho(r)$, for momentum transfer, q ,

$$F_c(q) = \frac{1}{(2\pi)^{3/2}} \int \rho(r) e^{-i\mathbf{q}\cdot\mathbf{r}} d\mathbf{r}.$$

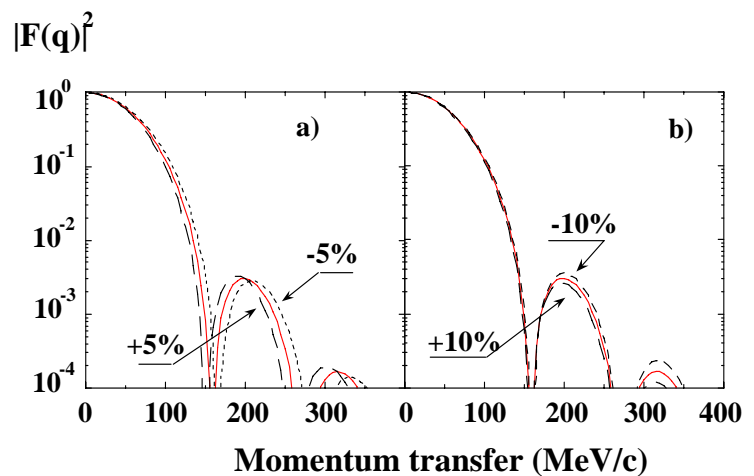


Fig. III-5-1. Result of a model calculation of the charge form factor for Sn. The parameters for the size and diffuseness in the Fermi distribution are changed for $\pm 5\%$, and $\pm 10\%$.

One determines $\rho_c(r)$ of a target nucleus by inverse Fourier transformation of the experimentally determined charge form factor. As is well known, there is a comprehensive data compilation of the charge form factor for stable nuclei obtained by elastic scattering [DE87].

Figure III-5-1 shows results of a model calculation for the charge form factor of the Sn isotope to demonstrate the sensitivity of the form factor to a change in the charge distribution. A Fermi-type distribution is assumed, and the parameters for the size and diffuseness are changed for $\pm 5\%$ and $\pm 10\%$, respectively. As can be seen in the figure, the dip position and the height of the diffraction maxima are found to have different sensitivities to the change of the distribution parameters.

By definition, the charge distribution, $\rho_c(r)$, can be determined model-independently, although one needs to measure the form factor up to infinite q . Practically, however, the form factor can be measured only in a finite q range in an experiment. The low luminosities, unavoidable for electron-RI scattering, will seriously hinder the measurement up to high-momentum transfer region due to nearly logarithmic reduction of the cross section as a function of q . Since our goal is to determine at least the size (radius) and shape (surface diffuseness) of the charge distribution, it is necessary to determine the dip position and the diffraction maximum of the form factor precisely as possible.

In the case of nuclei further from the stability line, whose production rate becomes less and less, the luminosity may be so low that the form factor is determined only for the lower q -region than that for the first diffraction minimum. One may still extract the r.m.s. charge radius, $\langle r_c^2 \rangle^{1/2}$, based on a model-independent relation of the form factor, $F_c(q)$, and $\langle r_c^2 \rangle^{1/2}$.

$$F_c(q) \sim 1 - \frac{\langle r_c^2 \rangle}{3!} q^2 + \dots$$

The required luminosity for an electron-RI scattering experiment is determined from the requirement that the charge form factor is necessary to be measured at least up to the first maximum.

In Fig. III-5-2, the expected yields of the elastic scattering events from ^{132}Sn are shown under the assumption of a luminosity of 10^{28} / cm^2/s , which is close to the maximum luminosity expected with this SCRIT concept as discussed before. The measurement is assumed to continue for one week. In the calculation, the electron energy is 300 MeV is assumed. As a detection system, a wide azimuthal angular coverage of $\pi/2$ is assumed, which will be discussed in III-5-2. From the figure, it is clear that the luminosity of an order of 10^{28} / cm^2/s is enough for electron scattering from the Sn isotope to cover the diffraction maximum in the charge

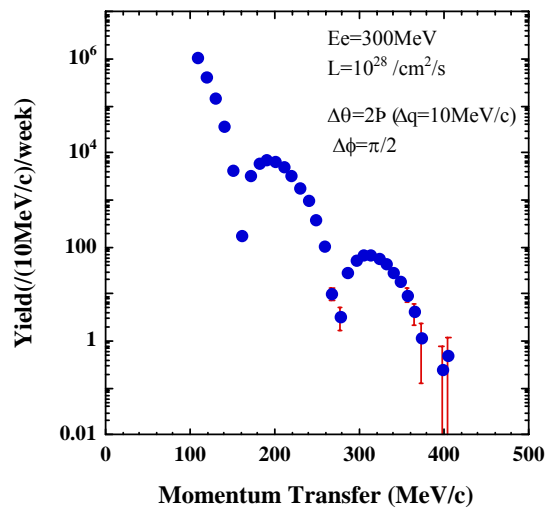


Fig.III-5-2 Expected yields for $^{132}\text{Sn}(e,e')$ in one-week measurement. It is assumed that the luminosity is 10^{28} / cm^2/s .

form factor with a reasonable measuring time of one week. If the assumed angular acceptance is realized, the measurement up to the first maximum of the form factor, which is the minimum requirement to determine the size and shape of a nucleus, can be performed even with the luminosity of $\sim 10^{26}$ /cm²/s.

III-5-2 Detector design concept

The main goal of this challenging project is, as repeatedly mentioned, the measurement of elastic cross section of electrons from short-lived nuclei, where the nucleus remains in its ground state.

As for the detection system, the conventional way is to employ a high-resolution spectrometer, an order of $\Delta p/p \sim 10^{-4}$ to achieve sub 100-keV energy resolution for a few 100 MeV electron beam energy, in order to resolve elastic and inelastic scattering. The price to pay for this high resolution is, of course, “small” solid angle, an order of a few msr to up to ~ 30 msr as the maximum solid angle, which has been realized in the modern electron spectrometers [BL98]. Since the cross section is necessary to be measured over a wide range of scattering angle to determine the form factor, the angular distribution must be measured by rotating the spectrometer around the target. This experimental method has been acceptable for such electron scattering experiments with fixed targets and intense electron beam.

In the case of electron-RI scattering, however, an extremely lower luminosity is foreseen. A detection system having a much larger solid angle is, thus, naturally demanded. Let us see large solid angle detectors currently under operation, such as BLAST [BL97] at MIT/Bates and CLAS [ME03] at JLAB. Those detectors are based on a technique to trace the electron trajectories inside solenoid or toroidal magnetic fields by tracking devices. Large angular acceptance with a wide scattering angular coverage and nearly full azimuthal angular coverage can be realized. A high resolution can not be, however, achieved due to unavoidable multiple scattering inside the tracking devices. A typical resolution is an order of sub %, which is not enough to identify the elastic scattering channel if one detects the scattered electrons only.

If one is interested in measuring only elastic-scattering cross section from short-lived nuclei, which may be sensible as *the first generation experiment*, the elastic scattering process can be identified by the kinematical coincidence between an electron and a recoiled nucleus. This is exactly true for nuclei having no (particle-bound) excited states, such as the deuteron. For nuclei having excited state, the identification of elastic scattering by the kinematical coincidence will be a good approximation if the (particle-bound) inelastic-scattering cross section is small enough compared to that of elastic scattering. The momentum transfer range of our interests is relatively low as 100-400 MeV/c, small contributions from the inelastic scattering cross section is a reasonable assumption for medium-heavy (stable) nuclei. If the contributions from inelastic scattering is also small in the case for short-lived nuclei, one can identify elastic scattering by detecting scattered electrons in coincidence with recoiled nuclei.

Thanks to ultra-thin RI target at rest realized by our novel SCRIT, the detection of recoiled nucleus becomes possible for the first time even under the momentum transfer range of 100 – 400 MeV/c. Therefore we are proposing to construct a detection system, which detects the scattered electrons in coincidence with the recoiled ions.

As a reference, a detection system planned at the electron-RI collider in the GSI future project is a high-resolution electron-spectrometer at the expense of solid angle. In the collider scheme, since it is not trivial to detect the recoiled ion under such a low momentum transfer, the detection of the scattered electron with a high-resolution spectrometer will be only a way. This is because of rather large momentum of the ion beam in the storage ring, the change of angle and/or momentum of the ion after scattering is generally too small.

In elastic scattering from a target nucleus at rest, the momentum of a recoiled nucleus is equivalent to the momentum transfer from an electron, which is purely determined by the electron scattering

$$q = 2E_e \sin\left(\frac{\theta}{2}\right),$$

kinematics. The momentum transfer to the target nucleus, q , is given by,

where E_e is the electron energy, θ the electron scattering angle. Since the electron beam energy E_e is fixed, the scattering angle, θ , determines the momentum transfer q . Knowing the recoil momentum to be q from the electron kinematics, one can determine the mass of the recoiled nucleus by measuring the time-of-flight (TOF).

The mass number, A , of the recoiled nucleus is, thus, related to q as,

$$q = Am_0 \frac{L}{T},$$

under the non-relativistic limit. This is a good approximation in our case because of very small recoil velocity ($\beta \ll 1$). Figure III-5-3 shows TOF for 10-cm flight path as a function of momentum transfer q for several elements. Here m_0 is the unit mass, L the flight path and T is TOF, respectively. The detection system must have at least the mass resolution, $\Delta A/A$, better than $1/A$ in order to confirm the mass of detected nucleus.

We have set $\Delta A/A$ to be better than $1/200$ in order to measure the elastic scattering cross section for medium mass nuclei, $A = 100-150$. In order to realize this mass resolution, the resolutions for

- (1) the electron scattering angle is $\Delta\theta = 1\text{mrad}$,
- (2) the TOF is $\Delta T = 1\text{ns}$ for the flight path of larger than 40 cm.

Here it is noted that typical recoil velocity of $A \sim 130$ nucleus is $10\text{ cm} / 100\text{ ns}$.

Figure III-5-4 shows the proposed detection system. The electron scattering angle of $30-90^\circ$ is covered with an azimuthal angular coverage of 90° . The solid angle is about 1.5

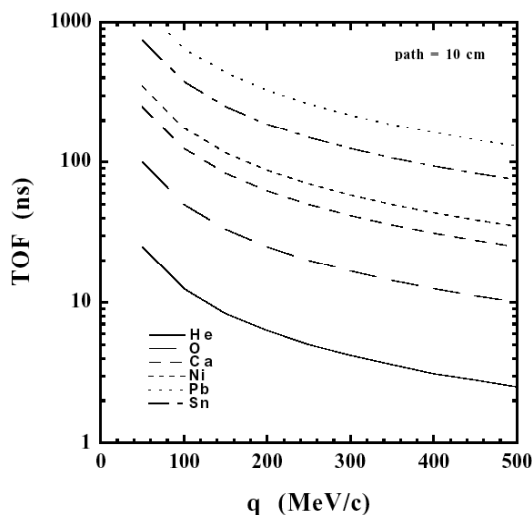


Fig.III-5-3. TOF for 10-cm flight path as a function of q .

sr, which is about two orders larger than the standard high-resolution magnetic spectrometers. The expected yields for ^{132}Sn with $L=10^{28}$ /cm²/s as shown in Fig. III-5-2 is based on this detector configuration.

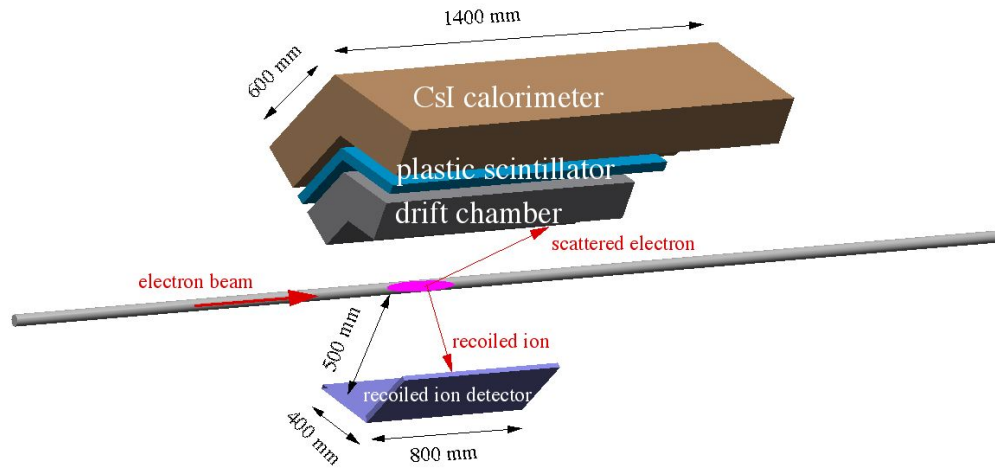


Fig.III-5-4. The conceptual drawing of the proposed detection system. The scattering angle of 30-90° and azimuthal angular coverage is 90°. The solid angle is 1.5 sr.

III-5-3 Electron Detection Arm

The detection of recoiled nucleus greatly relaxes restrictions for the electron spectrometers. Since the scattering angle of electrons is to be measured, a telescopic detection system can be now employed, as used in the SCRIT prototype at Kyoto KSR ring. The proposed electron detection system is based on a set of drift chamber, plastic scintillator and CsI calorimeters.

The electron detector is designed to cover the scattering angles of 30-90°. The momentum transfer range to be covered is set to be $q = 100 - 400$ MeV/c. Most of measurement will be done at a 300-MeV electron beam-energy, where the corresponding momentum transfer range is 150-400 MeV/c. In order to access lower momentum transfer around 100 MeV/c, the measurement at a 200-MeV electron beam energy will be performed. The maximum stored beam current for 200 MeV will be

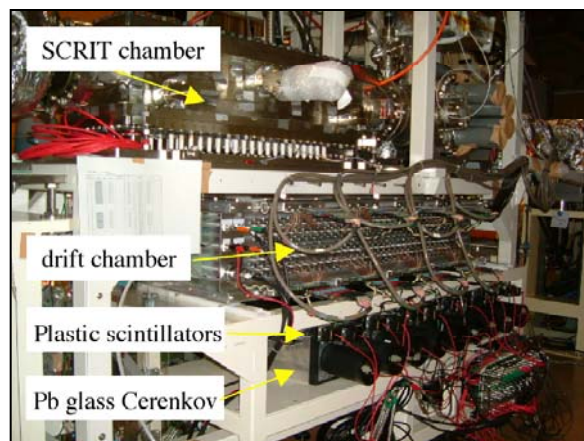


Fig. III-5-5. Electron detection system used in the KSR experiment. It consists of a drift chamber, plastic scintillators and calorimeters.

lower than that for 300 MeV, which results in lower achievable luminosity. The much larger cross section at lower energy, however, compensates the expected lower luminosity.

The electron detection system is placed outside the SCRIT vacuum chamber. The scattered electrons emerge from the vacuum chamber through a 1-mm Be window in order to minimize the multiple-scattering effect

Most of these detectors have been tested at the SCRIT prototype installed at KSR, and it has been confirmed that they function normally with the stored electron-beam current of 100 mA. Let us briefly summarize the detector system currently used in the KSR

experiment. Most of their parameters are being used for the proposed detection system. An electron detector consists of a drift chamber, 12 plastic scintillators and 9 calorimeters. Due to a geometrical limitation, the detection system has been installed below the SCRIT chamber, as shown in Fig.III-5-5. It is designed to cover scattering angles of 30-80°. With an electron beam energy of 100 MeV, the corresponding momentum transfer range is 50-130 MeV/c, as shown in Fig.III-5-6, where the elastic cross section dominates.

The electrons scattered at SCRIT are designed to pass through a 1-mm Be window of the SCRIT chamber to avoid multiple scattering.

The drift chamber has 128 hexagonal-shape drift cells, and the drift length is 18 mm. These cells are arranged so that at least 4 cells are fired for an electron track to reconstruct its trajectory. A premixed He+C₂H₆ (50:50) gas is used to make the chamber be insensitive as possible to low-energy photons originated from electromagnetic showers. The performance of the drift chamber has already been studied using cosmic rays, and background events during the test runs in the KSR experiments. As a result, a position resolution of 200 μm in r.m.s. has been achieved, which corresponds to a scattering angular resolution of a few mrad. During test runs with a stored electron beam of 80 mA, the drift chamber was confirmed to function normally.

Two layers of six plastic scintillators are placed under the drift chamber as a trigger system. The size of each scintillator is 200 x 300 x 10 mm³. A coincidence between two layers triggers data processing.

The total energy of the scattered electron is to be measured by 9 calorimeters. A Pb-glass Cerenkov detector is employed as a calorimeter, whose size is 340x122x135 mm³ [KA88]. Prior to installation, all detectors were energy-calibrated using a mono-energetic electron beam. Although the Pb-glass Cerenkov detector has a poor energy resolution, scattered electrons from the trapped ions under

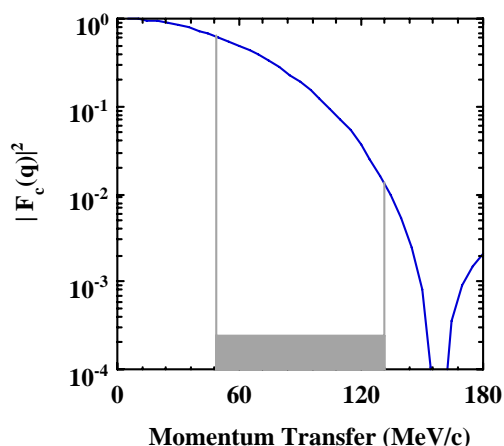


Fig. III-5-6. Momentum transfer region covered by the SCRIT prototype for $E_e = 100$ MeV.

the present kinematics can be safely assumed only from elastic scattering.

In the test experiment, this detection system function normally, although the elastic scattering events from the trapped ions in the SCRIT prototype is not yet confirmed. The detection system in the proposed system will be similar. CsI crystals will be employed as calorimeters, due to its fast response and much better energy resolution, instead of Pb glass Cerenkov detector. The length of a CsI crystal will be 25 cm, which corresponds to 15 radiation length. Typical energy resolution of CsI for 300-MeV electron is known to be 4 % (σ) [OK95].

III-5-4 Recoiled particle detector

The large acceptance of the SCRIT detection system will be realized with the recoiled-ion detection, where the kinetic energy of the recoiled ion is quite low. Measurement of heavy ions at such low energy down to 50keV level is a real challenge. There are no detection systems to date that are known to work sufficiently. Therefore we need to develop a detection method by ourselves to realize the electron-RI scattering experiments with SCRIT.

Recoil Arm Requirement

The recoil arm is located 50 cm away from the target region and covers 90 degrees azimuthally. Its length along the beam pipe is about 50 cm which corresponds to polar angle between 45 and 90 degrees. The energy of the recoiled nuclei ranges from 50 keV to 1 MeV. The recoil energy is so small that we have to place the recoil arm inside the very high vacuum (1×10^{-10} Torr) in the electron storage ring. It requires very stringent restriction to the choice of the detector since the system has to be baked up to 200 °C. Therefore we plan to use Micro Channel Plates (MCP) which are made of only bakable material namely metals and ceramics.

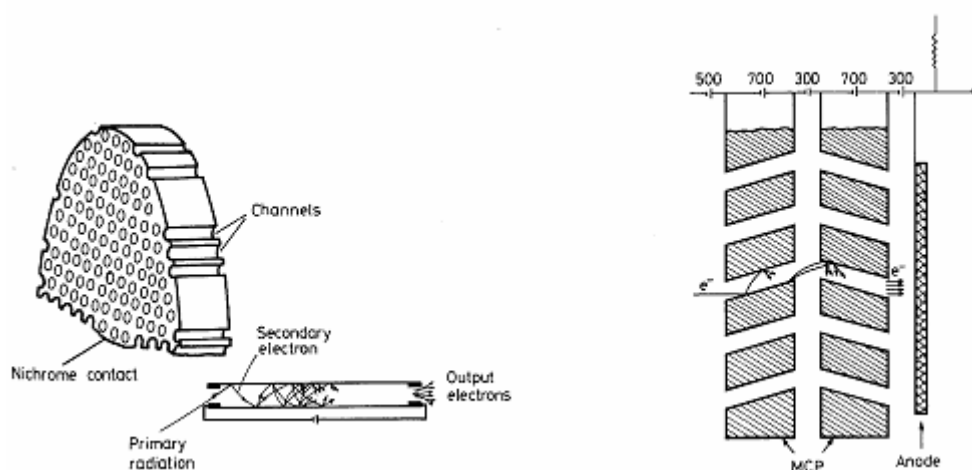


Figure III-5-7. Schematic diagram of MCP (left figure). Many channels act as continuous dynodes. To enhance the multiplication gain, multi-plate chevron configuration (right figure) is often used. [DAW75]

Figure III-5-7 shows the side view of the MCP. It consists of lead glass plate perforated by an array of microscopic channels oriented parallel to each other. The inner surfaces of the channels are coated with semiconducting material so as to act as secondary electron emitters while the flat end surfaces of the plate are coated with a metallic alloy so as to allow a potential difference to be applied along the length of the holes. The secondary electrons which are emitted by the primary radiation are thus accelerated along the hole until they eventually strike the wall to release further electrons. They repeat the same processes until the number of electrons becomes large enough to be readout by electronics. Each channel thus acts as a continuous dynode.

There are two ways to apply bias voltages (about 2kV) to the multiplication stage of the plate. One way is to apply negative high voltage to the front of the plate and connect the anode to the ground (negative biasing). The other way is to ground the front of the plate and apply positive high voltage to the anode (positive biasing). The former biasing scheme is favorable for ion detection since the ions are attracted by the negative potential on the front surface while electrons whose energy is less than 2kV are repelled. The latter scheme can be used for detection of both ions and electrons since the front potential is the ground.

Background Consideration

The beam pipe of electron storage rings is filled with synchrotron radiation, bremsstrahlung and stray electrons. Those electrons are generated by several physics processes between beam electrons and surrounding materials including residual gas and beam pipes. Such processes include Moller scattering, electromagnetic showers, Compton scattering, photoelectric effect and secondary electron emission from the beam pipe surfaces. Since MCP is sensitive to electrons, we need to consider how to avoid the background electrons.

Due to the fact that the background electrons are generated by so many processes, it is difficult to perform a reliable simulation to estimate the abundance and the energy spectrum of them. Therefore we installed two MCP in the KSR ring approximately 50 cm away from the beam line and we plan to measure the electron spectra during the next test experiment which is scheduled in the late fall 2005.

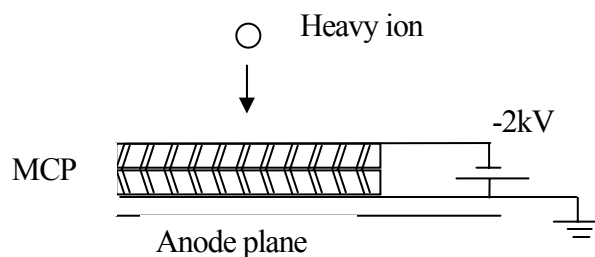


Figure III-5-8. Schematic view of the configuration I. MCP front surface is kept at negative potential.

Detector Configuration

Configuration I:

The most straightforward approach is to accept the recoiled nuclei directly by MCP. As shown in Figure III-5-8, the front of the MCP is kept at negative potential so that the recoiled nuclei (most likely

charged heavy ions) are attracted there. On the other hand, the background electrons whose kinetic energy is less than the potential energy (typically $\sim 2\text{keV}$) are repelled from the front surface of the sensitive volume.

Among all the physics processes which generate electrons, electromagnetic shower is

considered to be the primary source. From the geometry of the KSR accelerator, we consider the background shower electrons whose energy is more than 2keV has tolerable event rate (several kHz). More accurate estimation of the electron background rate will be performed by a computer simulation and an actual electron energy spectrum measurement.

The drawback of this configuration is that the pulse height of the recoiled nuclei is expected to be the same as that of single electrons. It is because the multiplication of the electrons to its saturation current occurs at one hole of MCP. If it turns out to be a significant problem, a thin carbon foil (thickness $\sim 5 \mu\text{g}/\text{cm}^2$) may be placed in front of MCP with negative potential applied. This configuration allows heavy ions to emit tens of atomic electrons from the foil. The foil acts as a preamplifier of the incident charge and works as an electron repeller at the same time. With this option, the positive biasing has to be applied to MCPs instead of negative biasing.

Configuration II:

If the background electron rate turns out to be too high for MCP to face the target region directly, we reserve an option to detect recoiled nuclei indirectly via secondary electron emission on a metal surface. MCP can be placed somewhere free from the direct exposure to the background electrons as shown in Figure III-5-9. When 50keV or above heavy ions enter a surface of a metal, tens of secondary electrons are emitted from the surface. Those electrons can be accelerated away from the surface using a potential mesh plane and guided onto the MCP sensitive surface utilizing electric field. This configuration requires more elaborate geometrical arrangement but it is much more robust against the background electrons.

III-5-5 Luminosity Monitor

The luminosity is continuously monitored by observing bremsstrahlung at downstream of the SCRIT chamber. The bremsstrahlung process is a reliable way for the luminosity monitoring, since the

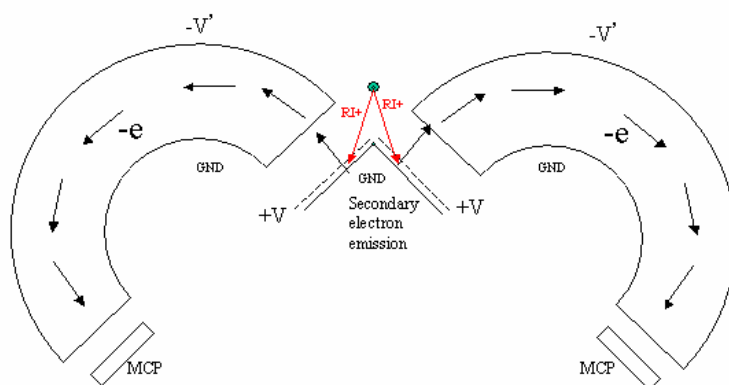


Figure III-5-9. Schematic view of the configuration II. MCP is hidden from the direct exposure to the electrons. Secondary electrons that are emitted at the surface of metal plates are guided to MCP

cross section is precisely known, and large. Note that the cross section has the Z^2 dependence and is ultra-forward peaked, $\theta_\gamma \sim m_e/E$.

The luminosity monitor consists of optically-isolated seven (pure) CsI crystals. Each crystal has a hexagonal cross section with a diameter of 7 cm, and a length of 25 cm (15 radiation length). A thin plastic scintillator is placed in front of the CsI detector for charged-particle veto. A pair of collimators with 10-mm diameter is placed in front of the CsI detector to remove background, and to restrict the γ -ray irradiation only to the central crystal. The expected counting rate for ^{132}Sn with $L = 10^{28}/\text{cm}^2/\text{s}$, as an example, is 200 kHz for $E_\gamma \geq 20$ MeV.

The similar type of the luminosity monitor, not CsI but BaF_2 crystal, is currently used at the KSR experiment. In order to achieve high counting-rate capability, CsI crystals having much shorter decay constant will be employed.

In order to reduce the background bremsstrahlung from the residual gas, electrodes as trapped ion clearer must be installed for the straight section where the SCRIT chamber is placed. From our experience at the KSR experiment, the background bremsstrahlung due to residual gas is more than one order larger than expected from the vacuum. This has been attributed to higher residual gas density on the electron beam due to the ion trapping effect. The ion clearers remove the trapped residual gas ions from the electron beam.

As an additional monitor, the detection of characteristic X-ray from the trapped ions is now tested at the prototype experiment. The characteristic X-ray is emitted from the target nuclei when an innermost electron of an ion is knocked out by high-energy electron beam through Moeller scattering. The energy of the characteristic X-ray of Sn is about 25 keV, which is detectable by a Ge detector. The emission of the characteristic X-ray is a direct evidence of the spacial overlap between electron beam and trapped ions. Since the Moeller cross section is large, an order of 100 b, one expects about 10^6 characteristic X-rays for a luminosity of $10^{28}/\text{cm}^2/\text{s}$, which will be emitted in 4π , though. A Ge detector will view the target region through a Be window. The detection of such a low energy X-ray is possible in this SCRIT scheme due to ultra-thin target at rest. The feasibility of this method is now under study at the SCRIT prototype.

In order to increase the reliability of the luminosity determination, the Moeller monitor and a monitor for measuring ultra-forward scattered electron are discussed.

- (1) The Moeller scattering process, whose large cross section has Z^1 -dependence, at $\theta_{\text{CM}}=90^\circ$ produces a symmetric electron pair in the final state at $\theta_{\text{lab}}=3.3^\circ$.
- (2) Since the cross section for elastic scattering at ultra-forward angles is huge due to its $1/\sin^4(\theta/2)$ dependence, this is alternative way to monitor the luminosity accurately.

The feasibility of these additional luminosity monitor will be tested at the KSR experiment.

III-6. Further recycling plan

For further reduction of the construction cost, we are now studying about recycling of the KSR and its injector linac, which we are now using in the R&D study. Since the acceleration energy of the linac is

100 MeV, we do not need to buy an injector microtron described above. By using parts of the KSR such as magnets, power supply, control system, etc., renewals these parts of the NIJI-II are also unnecessary. The beam power of the linac for the KSR injection is not enough to use for RI production. But we can raise a construction cost for high-power 50-MeV electron linac with this further recycling plan. The plan view with the KSR recycling, which has the highest cost performance, is shown in Fig. III-6-1

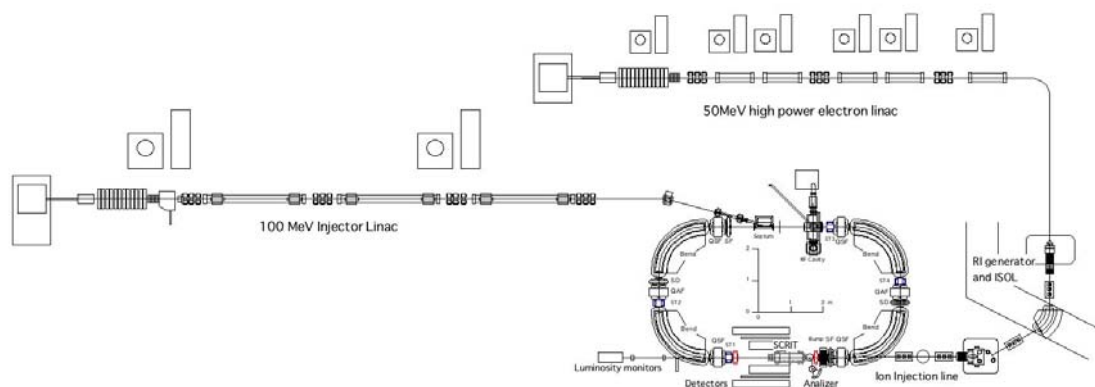


Fig.III-6-1. Plan view with the KSR recycling.

IV. R&D STUDY OF THE SCRIT

In the R&D study, which is now under way at the KSR in Kyoto University, we confirmed that the ^{133}Cs ions are trapped in the SCRIT, and the feasibility of the SCRIT as a target is expected to be high. Here we report status of the R&D study and preliminary results of ion trapping in the SCRIT.

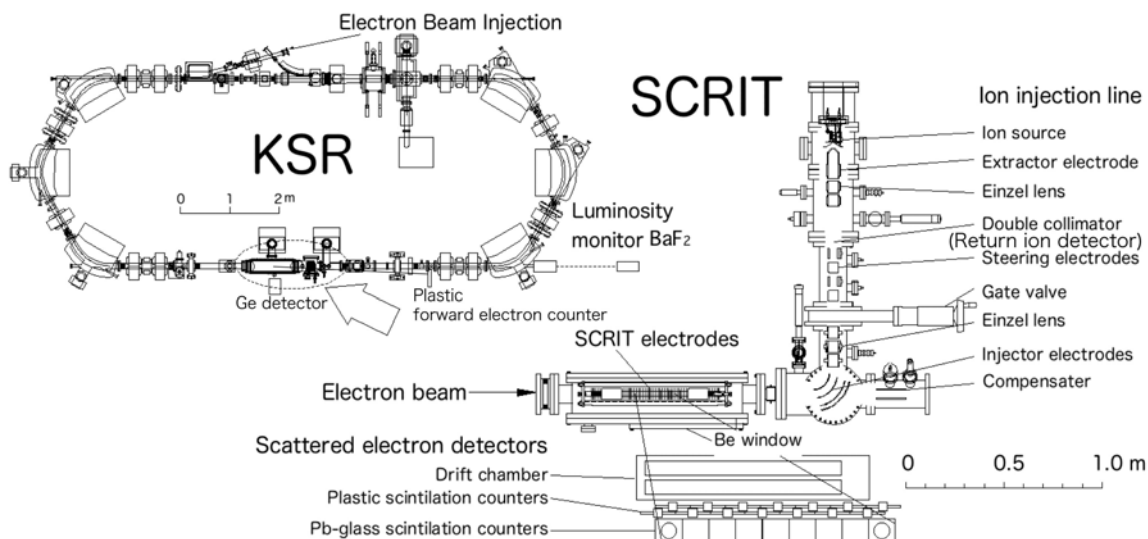


Fig. IV-1-1. R&D prototype of the SCRIT installed into the KSR.

IV-1. Prototype of the SCRIT device

A prototype of the SCRIT devices is installed into the KSR [NO96] as shown in Fig. IV-1-1. The KSR is the racetrack type of the storage ring adopting the TBA lattice structure. An electron beam energy is 100 MeV and its current is 80-90 mA in our experiment. The prototype consists of the SCRIT device, an ion source, and an electrostatic transport line for ion injection. The surface ionization ion source of ^{133}Cs is used and the pulsed ion beam is generated by grid action. Ion beam accelerated to 10 keV and merged with the electron beam axis by the 90-degree deflector. The SCRIT is the electrode system, in which 40-thin electrodes are stacked every 11 mm, to make a longitudinal mirror potential. The potential wall is quickly switched off and its timing is synchronized to the ion injection. Figure IV-1-2 shows photographs of the SCRIT device.

In order to detect scattered electrons, a drift chamber, plastic scintillators, and calorimeters are set under the SCRIT chamber. They are for the ray trace, the event trigger, and the total energy measurement. Another plastic scintillator used for cosmic ray veto are put above the SCRIT chamber. Three kinds of luminosity monitors are prepared. The BaF_2 scintillators are placed at the downstream of the SCRIT to detect the bremsstrahlung whose intensity is expected to be enhanced by the trapped ^{133}Cs ions. A plastic scintillator to detect forward scattered electrons is set at the Moeller scattering kinematics for $\theta_{\text{CM}}=90^\circ$. And a Ge detector to measure the characteristic X-ray from Cs ions induced by electron beam impact. Details of the detectors are described in section III-5.

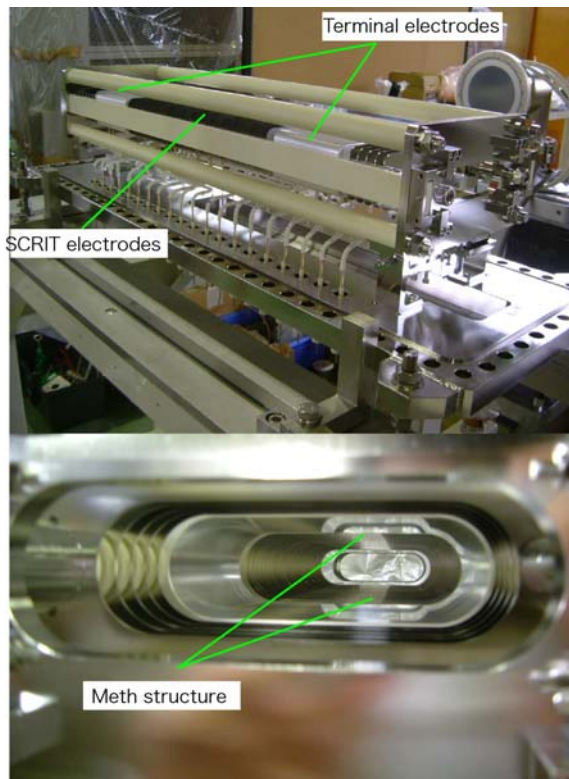


Fig. IV-1-2. Photographs of the SCRIT device.

IV-2. Measurements of Cs ion trapping in the SCRIT

Trapping of the ^{133}Cs ions in the SCRIT was confirmed by means of measurement of the released ions from the SCRIT at a certain trapping time after injection. Released ions go back along the injection line and a part of them was detected at a returned-ion detector. Taking the efficiency and the estimation of the average charge state into account, the number of Cs ions trapped in the SCRIT is obtained, and this is plotted as a function of the trapping time in Fig. IV-2-1. In this figure, the average charge state estimated at vacuum pressure of 10^{-7} Pa is also plotted. Four series plotted in the figure have different number of

initially injected ions (N_{inj}). In case of large number of N_{inj} , trapped ions decreased much faster. This is the expected in the calculation shown in Fig. III-1-3. Assuming that the ions exist transversely inside the electron beam envelope in the SCRIT, the luminosity can be calculated to be $L \sim 10^{24} \text{cm}^{-2} \text{s}^{-1}$ in the trapping-time region of 0.1~1s, $L \sim 10^{25} \text{cm}^{-2} \text{s}^{-1}$ in 10~100ms, and $L \sim 10^{26} \text{cm}^{-2} \text{s}^{-1}$ in 1~10ms.

It was found in this measurement that the number of trapped ions strongly depends on the electron-beam current. Figure IV-2-2 shows that for Cs ions and residual gas ions. These data are measured at fixed trapping time, which is 1s for residual gas ions and 0.5ms for Cs ions. Green lines in the figure indicate the neutralization of 3, 10, 30, and 100%, and red dashed lines show a luminosity of 10^{27} and $10^{28} \text{cm}^{-2} \text{s}^{-1}$. From this figure, we can easily realize that the required luminosity can be achieved at several hundreds mA.

Unfortunately we have not yet succeeded to observe direct evidences of the interaction between the trapped ions and the electron beam, which are the enhancement of bremsstrahlung, enhancement of forward scattered electrons, and characteristic X-ray due to the knockout process of the innermost electrons. The reason is that the events from the processes mentioned above is smaller than those due to background. We know how to reduce the background and improvements for that is now under way at the KSR.

Presently we confirm that the Cs ions injected from outside are trapped in the SCRIT with controllable lifetime, and the SCRIT is feasible as a target for the electron scattering. After improvements with respect to reduction of the background, we will try to directly measure the luminosity and make electron scattering experiment for the stable Cs ions. This can demonstrate the feasibility of the new electron scattering system with the SCRIT.

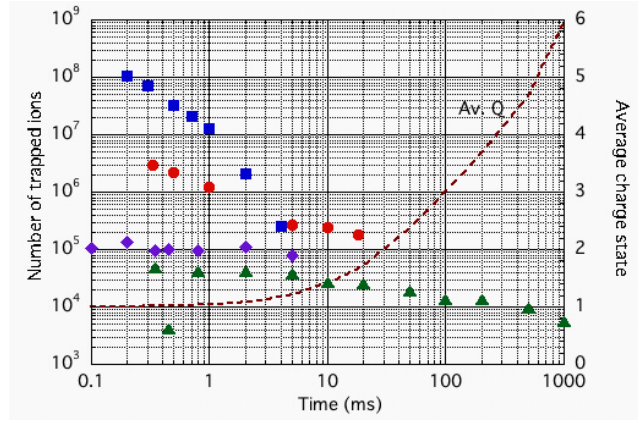


Fig. IV-2-1. Number of trapped Cs ions in the SCRIT.

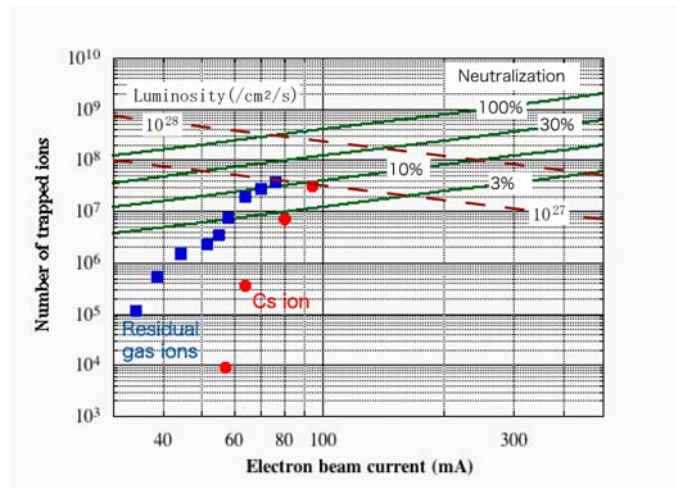


Fig. IV-2-2. Electron-beam current dependence of number of trapped ions.

V. COSTS

V-1. Cost of the minimum plan

In case of the minimum plan without any options for RI generation shown in Fig. III-2, estimated construction costs are follows.

Table V-I-1. Cost of the electron accelerator (unit Myen)

Microtron	Whole system	500
Total cost of injector		500

Table V-I-2. Cost of the storage ring based on modifying of the NIJI-II (unit Myen).

Storage ring	Additional vacuum system	15
	Additional steering magnets and beam monitors	10
	Renewal of power supplies of magnets	30
	The renewal of control system	50
	The renewal of rf power source	50
	The SCRIT device	50
	Dismantlement, transportation and reconstruction	20
Total cost of the storage ring		225

Table V-I-3. Cost of the RI generator, ISOL , and ion injection system (unit Myen)

ISOL	RI generator	20
	Mass separator and transport	20
	Shield	30
Ion injection system	Pulse ion source	10
	Transport line to the SCRIT	10
Total cost of RI generator and injector		90

Table V-I-4. Cost of the spectrometer and detectors. (unit Myen)

Detector system	Electron detector	180
	Recoiled ion detectors	100
	Luminosity monitor	20
Total cost of the detection system		300

Total cost of the electron scattering experiment (the minimum plan): 1,115 Myen.

V-II. Cost of additional high-power electron linac for RI production

If we chose the high-power electron linac as a driver of the RI production, additional costs are

follows.

Table V-II-1. Cost of the high-power linac. (unit Myen)

Production linac	10MeV Accelerating structure (5units)/gun/ prebuncher /buncher	80
	RF modulator and power supply (5units)	305
	Magnet and power supply	15
	Microwave components (circulator etc.)	50
	Beam instrumentation (BPM, current monitor etc.)	10
Control	Low level RF and control system	10
Vacuum system		15
Magnet	Switch and transport arcs	20
RI generator	Renewal for the UC ₂ target	100
	Radiation shield	50
Total cost of the linac		655

Table V-II-2. Cost of the improvement of the RI generator for use of UC₂ target. (unit Myen)

RI generator	Radiator, Target, Ionizaer	20
	Radiation shield	30
Total cost of the improvement		50

Total cost including the minimum plan shown in section V-I: 1,820 Myen.

V-III. Cost of full specification with recycling of the KSR and its injector linac

The cost of the construction of full specification shown in Fig. III-6-1 with recycling of the KSR and its injector linac is estimated as follows.

Table V-III-1. Cost of the electron accelerator (unit Myen)

KSR injector	Dismantlement, transportation and reconstruction	50
Total cost of injector		50

Table V-III-2. Cost of the storage ring based on recycling of the KSR and the NIJI-II (unit Myen).

Storage ring	Additional vacuum system	15
	The renewal of control system	20
	The SCRIT device	50
	Dismantlement, transportation and reconstruction	20
Total cost of the storage ring		105

In addition to these costs, the RI source (Table V-I-3), the detector system (Table V-I-4), and the driver linac for RI production (Table V-II-1) must be included for full specification system.

Total cost of the electron scattering experiment (full specification): 1,200 Myen.

VI. TIME TABLE OF CONSTRUCTION, BUDGETS, AND STAFFS

The timetable of the construction and staff plan are shown in the next table. This timetable is for the case of full specification system with the recycling of the KSR and its injector linac.

The construction is scheduled to be performed in the year 2008-2010. Depending on the R&D results currently underway at KSR, however, the time schedule will be changed. The feasibility of this novel SCRIT method for electron-RI scattering is shown by this R&D, the detailed design of the machine, RI generator and detection system will be immediately started. In addition, calling for collaborations will be necessary.

		2005	2006	2007	2008	2009	2010	
R&D study		R&D at KSR →						
Construction	Electron beam injector				Move to RIKEN	Reconstruction	Operation	
	Storage ring				Design study	Move to RIKEN	Reconstruction	Operation
	High-power electron linac				Design study	Construction	Operation	
	RI generator and injection system				R&D and Design study	Construction	Operation	
	Detector system				R&D and Design study	Construction	Operation	
Construction Budget	Total 1,130 (Myen)				130	500	500	
Staff plan	Electron beam injector	0	0	1	1 + Ph.D 1	1 + Ph.D 1	1 + Ph.D 1	
	Storage ring	2	2	2	2	2 + Ph.D 1	2 + Ph.D 1	
	High-power electron linac	0	1	1	1 + Ph.D 1	1 + Ph.D 1	1 + Ph.D 1	
	RI generator and injection system	0	1	1	1	1 + Ph.D 1	1 + Ph.D 1	
	Detector system	1	2	2	2 + Ph.D 1	2 + Ph.D 1	2 + Ph.D 1	
	Total staff	3	5	6	7 + Ph.D 3	7 + Ph.D 5	7 + Ph.D 5	

References

- [AL99] G.D. Alton, J.R. Beene, and Y. Liu, Nucl. Instrum. Meth., **A438**, 190 (1999).
- [AR76] J. Arianer and C. Goldstein, IEEE Trans. Nucl. Sci., **NS-23**, 979 (1976).
- [BA86] M.Q. Barton, Nucl. Instrum. Meth., **A243**, 278 (1986).
- [BL97] BLAST Technical Design Report, Bates Linear Accelerator Center, 1997
- [BL98] K. I. Blomqvist *et al.*, Nucl. Instrum. And Method, **A403** (1998) 263.
- [BO89] C.J. Bocchetta and A. Wrulich, Nucl. Instrum. Meth., **A278**, 807 (1989).
- [DA75] S. Dahwan, R. Majka IEEE Trans.Nucl.Sci.Ns-22 No.1 (1975) 303-305
- [DE66] T. deForest Jr., J. D. Walecka, Adv. In Phys. 5(1966)1.
- [DE87] H. de Vriese, C. W. de Jager and C. de Vries, Atom. Data Nucl. Data Tables, 36(1987)495.
- [DI99] W.T. Diamond, Nucl. Instrum. Meth., **A432**, 471 (1999).
- [DO76] E.D. Donets, IEEE Trans. Nucl. Sci., **NS-23**, 897 (1976).
- [KA88] S. Kawabata *et al.*, Nucl. Instrum. And Method, **A270** (1988) 11.
- [LA74] L.J. Laslett, A.M. Sessler, and D. Möhl, Nucl. Instrum. Meth., **121**, 517 (1974).
- [ME03] B. A. Mecking *et al.*, Nucl. Instrum. And Method, **A503** (2003) 513.
- [NO96] A. Noda, *et al.*, Proc. of 5th Int. Conf. of European Particle Accelerator Conference, Barcelona, p451 (1996).
- [OK95] H. Okuno *et al.*, Nucl. Instrum. And Method, **A365**(1995)352.
- [PE91] B.M. Penetrante, *et al.*, Phys. Rev., **A43**, 4861 (1991).
- [SU05] T. Suda and M. Wakasugi, Prog. Part. Nucl. Phys. **55**, 417 (2005).
- [TA95] I. Tanihata, Nucl. Phys., **A588**, 253c (1995).
- [TA03] H. Takeda, *et al.*, AIP Conf. Proc. **675**, p720 (2003).
- [WA04] M. Wakasugi, T. Suda, and Y. Yano, Nucl. Instrum. Meth., **A532**, 216 (2004).
- [WE01] R.F. Welton, *et al.*, Proc. of 16th Int. Conf. of Application of Accelerator in Research and Industry, p250 (2001).
- [YA04] Y. Yano, Proc. of 17th Int. Conf. of Cyclotrons and Their Applications, Tokyo, Japan, p169 (2004).